# Simulations of ITER, FIRE, and IGNITOR Using the BALDUR Integrated Predictive Modeling Code

Glenn Bateman, Thawatchai Onjun, Arnold H. Kritz,
and Alexei Pankin

Lehigh University Physics Department
16 Memorial Drive East
Bethlehem, PA 18015

Contribution to the 2002 Snowmass Meeting

25 June 2002

## Abstract

The Multi-Mode transport model [1] is used together with new models for the height of the pedestal at the edge of H-mode plasmas [2,3] in the BALDUR integrated predictive modeling code [4] to predict the performance ITER, FIRE, and IGNITOR fusion reactor designs.

## Introduction

Integrated modeling simulation codes have been developed to predict the time evolution of the plasma temperature, density, and other profiles in tokamak plasmas [1,5]. These integrated modeling codes compute the sources, sinks, and transport of thermal and particle energy densities, as well as the equilibrium shape of the plasma and the effects of large-scale instabilities [4]. The results of these simulations have been compared with experimental data from a wide range of tokamak discharges [5,6].

Before this year, experimental data was used to provide the temperatures and densities at the outer boundary of integrated modeling simulations of tokamaks. Models were needed for the boundary conditions in order to make the integrated modeling codes more completely predictive. In particular, in the case of fusion reactor scenarios involving H-mode plasmas, it was known that the predicted performance of fusion reactor designs (*ie*, the predicted fusion power production) depended sensitively on the temperature and density at the top of the pedestal at the edge of the H-mode plasmas. Models have recently been developed and calibrated against experimental data to predict the temperature and density at the top of the pedestal at the edge of the H-mode plasmas [2,3]. The results of simulations using these models for the H-mode pedestal together with models for the core plasma transport, sources, and sinks, have been compared with experimental data for the temperature and density profiles [3].

In this report, a combination of core and pedestal models is used in the BALDUR integrated predictive modeling codes to simulate fusion reactor designs and to predict their performance.

## H-mode Pedestal Models

Models are developed to predict the temperature and density at the top of the pedestal at the edge of type 1 ELMy H-mode plasmas in order to provide the boundary conditions needed for integrated predictive simulations1. In the model presented here, the width of the temperature pedestal, Δ, is assumed to be determined by a combination of magnetic and flow shear stabilization of drift modes [7], $\Delta = C_W \rho s^2$, where $s$ is the magnetic shear, $\rho$ is the ion gyro-radius and $C_W$ is a constant of proportionality chosen to optimise the agreement with experimental data. A constant pressure gradient, limited by the ideal MHD ballooning mode limit, is assumed so that the normalized critical normalized pressure is given by

$$\alpha_c \equiv -2\mu_o R q^2 (\partial p / \partial r)_c / B^2 = 0.4 s (1 + \kappa_{95}^2 (1 + 5\delta_{95}^2)), \quad [1]$$

where the magnetic $q$ and shear $s$ are evaluated one pedestal width away from the separatrix; $R$ is the major radius, and $B$ is the toroidal magnetic field. The dependence of $\alpha_c$ on elongation and triangularity at the 95% magnetic flux surface, $\kappa_{95}$ and $\delta_{95,}$ is described by the geometrical factor included in Eq. (1). The pedestal pressure is the product of the pedestal width times the critical pressure gradient, which, after some algebra results in the following expression for the pedestal temperature:

$$T_{\text{ped}}[\text{keV}] = 1.89 C_W^2 \left(\frac{B}{q^2}\right)^2 \left(\frac{M_i}{R^2}\right) \left(\frac{\alpha_c}{n_{\text{ped}\,19}}\right)^2 s^4, \quad [2]$$

where $n_{\text{ped }19}$ is the electron density at the top of the pedestal in units of $10^{19}$ $m^{-3}$.

The magnetic $q$ has a logarithmic singularity at the separatrix and it is a function of plasma elongation and triangularity near the edge of the plasma. At one pedestal width away from the separatrix, the magnetic $q$ is approximated by

$$q = \frac{0.85 a^2 B}{I_{\text{MA}} R} \frac{1 + \kappa_{95}^2 (1 + 2\delta_{95}^2 - 1.2\delta_{95}^2)(1.17 - 0.65 a/R)}{[1 - (a/R)^2]^2} \left[ \left(1 + \left(\frac{r}{1.4R}\right)^2\right)^2 + 0.27 \left| \ln\left(\frac{1-r}{a}\right) \right| \right], [3]$$

where $r = a - \Delta$ is the position of the top of the barrier [2]. The magnetic shear, $s = (1/q)(\partial q / \partial r)$ is computed using Eq. (3) and is then reduced by the effect of the bootstrap current. Since the pedestal width is needed to compute the magnetic $q$, $s$, and $\alpha_c$, and since the pedestal width is a function of the pedestal temperature, the right side of Eq. (2) depends nonlinearly on the pedestal temperature, $T_{\text{ped}}$ and a non-linear equation solver is required to determine $T_{\text{ped}}$.

The coefficient $C_W$ in the expression for the pedestal width is determined by calibrating the model for the pedestal temperature against 533 data points for type 1 ELMy H-mode plasmas obtained from the International Pedestal Database version 3.1 (http://pc-sql-server.ipp.mpg.de/Peddb/) using discharges from ASDEX-U, DIII-D, JET, and JT-60U tokamaks. It is found that the value $C_W = 2.42$ yields a minimum logarithmic RMS deviation of about 32% for this data. The comparison between the pedestal temperature from this model and experimental data is shown in Fig. 1. It is found that a simple empirical expression for the pedestal density $n_{ped} = 0.71\bar{n}$, where $\bar{n}$ is the line-averaged plasma density, results in a pedestal density that fits the 533 data points with a logarithmic RMS deviation of 12%, as shown in Fig. 2.

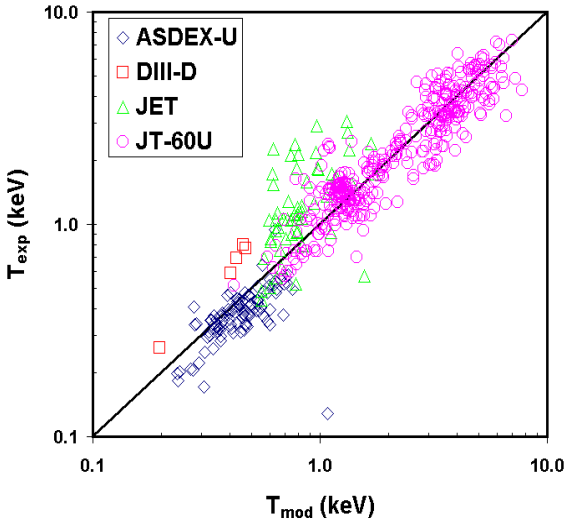


*Figure 1: Predicted pedestal temperature compared with 533 experimental data points from the*

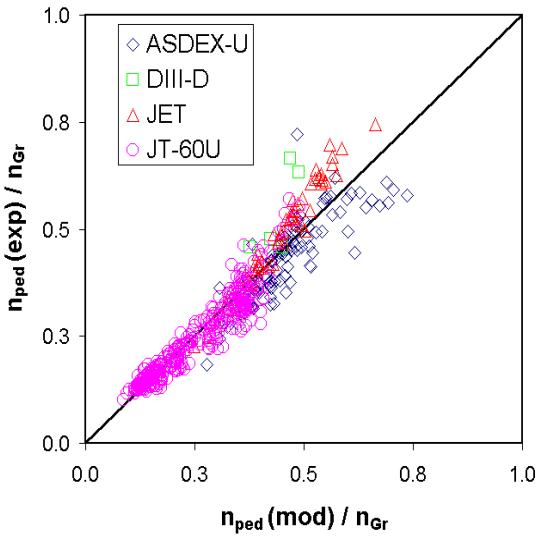


*Figure 2: Predicted pedestal density compared with 533 experimental data points, normalized by the Greenwald density.*

If the coefficient in this model, $C_W$, is taken to be 2.42, then half the data points lie below the model and half lie above the model in Fig. 1. As the coefficient, $C_W$, is varied, the fraction of data points that lie above the model changes as shown in Fig. 3. In order to estimate the range of variation needed to cover one standard deviation above and below the model, we sweep $C_W$ through a range of values that cover 34% of the data points above and below the standard model. That is, if we increase $C_W$ to 4.86, we find that 34% of the data points lie between the standard model and this upper bound. If we decrease $C_W$ to 1.16, we find that 34% of the data points lie between the standard model and this lower bound.

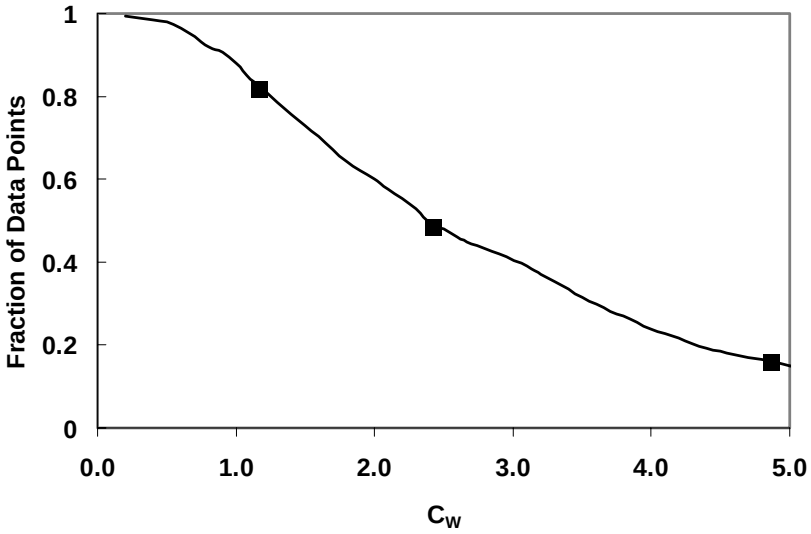


*Fig. 3: Fraction of experimental data points with pedestal temperature larger than the pedestal temperature predicted by the model as a function of the coefficient in the pedestal width $C_W$. Solid points indicate the standard model ($C_W$=2.42) as well as one standard deviation above ($C_W$=4.86) and below ($C_W$=1.16) the standard model.*

The model for the pedestal temperature, described above, is used to provide the boundary conditions in simulations of H-mode discharges in the BALDUR integrated predictive modeling code. The standard Multi-Mode model [3] is used as the core transport model in these simulations. It is found that the overall agreement between the simulated profiles and experimental data when the model is used to predict the edge temperature and density is of the order of 10%, which is comparable to the results obtained when experimental values are used to provide the boundary conditions in the simulations. In Figures 4 and 5, results obtained from simulations using the pedestal model for $T_{ped}$ are compared with experimental data for the profiles in 12 H-mode discharges.

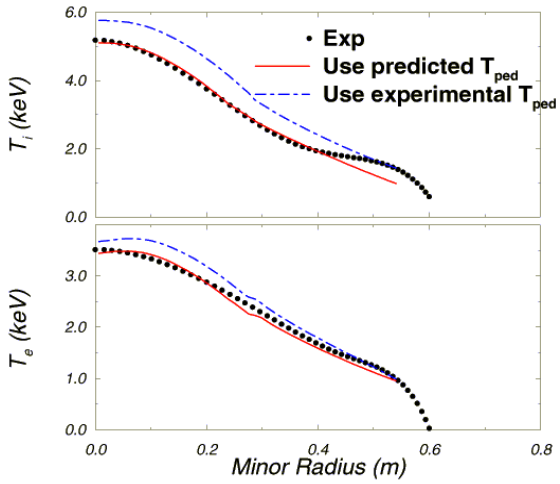


*Figure 4: Example of simulation results compared with experimental data for $T_i$ and $T_e$ profiles in DIII-D 81321 using predicted or experimental values for $T_{ped}$.*

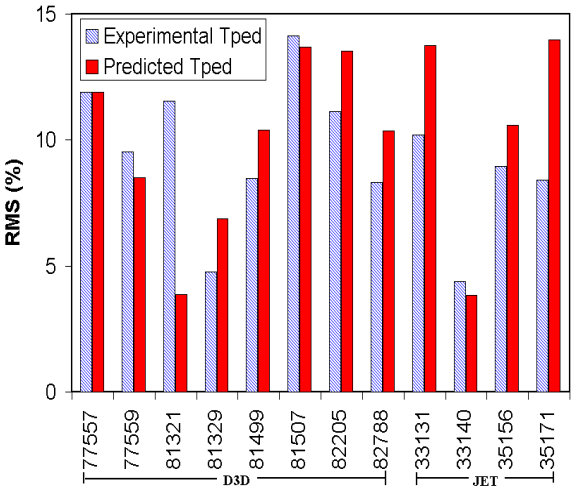


*Figure 5: The RMS deviation between the simulation results for the $T_i$ profiles and the experimental $T_i$ profiles for eight DIII-D and four*

## Simulations of ITER, FIRE, and IGNITOR

The pedestal model was then applied to simulations of ITER, FIRE, and the H-mode scenario in IGNITOR. The design parameters used in these simulations are given in Table I. The parameters given in this table are the major radius, $R$ m, the minor radius (*ie*, the half-width to the edge of the simulation), $a$ m, the toroidal plasma current, $I_p$ MA, vacuum toroidal magnetic field at major radius $R$, $B$ tesla, the plasma elongation at the edge of the simulation, $\kappa_{95}$, the plasma triangularity at the edge of the simulation, $\delta_{95}$, the Greenwald density limit, $n_{Greenwald,20} = I_p/(\pi a^2)$, the average electron density divided by the Greenwald density, $\langle n_e \rangle / n_{Greenwald}$, the volume-averaged electron density, $\langle n_{e20} \rangle$ in units of $10^{20}$ $m^{-3}$ for the reference design point, the pedestal electron density for that volume-averaged density, $n_{ped,20}$, the pedestal temperature from the model described in the previous section for that pedestal density, $T_{ped}$ keV, the power needed for the transition from L-mode to H-mode, $P_{L\rightarrow H}$ MW, and a description of the impurity concentration used in the simulation, not including the Helium that accumulates due to fusion reactions (which was typically 2% or less).

Table I: Plasma parameters used in the simulations of ITER, FIRE, and IGNITOR.

| | **ITER** | **FIRE** | **IGNITOR** |
|---|---|---|---|
| $R$ **m** | 6.2 | 2.14 | 1.32 |
| $a$ **m** | 2.0 | 0.595 | .45 |
| $I_p$ **MA** | 15.0 | 7.7 | 9.0 |
| $B$ **tesla** | 5.3 | 10 | 13.0 |
| $\kappa_{95}$ | 1.7 | 1.77 | 1.83 |
| $\delta_{95}$ | 0.33 | 0.4 | 0.4 |
| $n_{Greenwald,20}$ | 1.19 | 6.92 | 14.2 |
| $\langle n_e \rangle / n_{Greenwald}$ | 0.84 | 0.7 | 0.6 |
| $\langle n_{e20} \rangle$ | 1.0 | 4.85 | 8.5 |
| $n_{ped,20}$ | 0.71 | 3.44 | 6.0 |
| $T_{ped}$ keV | 2.74 | 2.34 | 2.22 |
| $P_{L \rightarrow H}$ **MW** | 48.5 | 26.4 | 22.3 |
| **Impurity** | 2% Be + 0.12% Ar | 3% Be | 1.7% Be |

Note that in the simulations of IGNITOR design, the plasma current is taken to be 9 MA rather than the full design current of 11 MA. It is predicted that a separatrix forms with an X-point inside the vacuum vessel at the reduced current of 9 MA, while the plasma is limited by the vacuum vessel at the full current of 11 MA [8]. It is more likely that an H-mode of the kind predicted by our models will be produced in a plasma that has a separatrix with the X-point inside the vacuum vessel than in a plasma that is limited by the vacuum vessel. Hence, the reduced plasma current scenario is used in our simulations in order to provide a uniform basis of comparison in which all three fusion reactor designs were simulated with the same kind of H-mode plasma.

It can be seen in Fig. 6 that the predicted pedestal temperature is inversely related to the pedestal density. In this figure, the density is normalized by the Greenwald density, $n_{Gw} = I_p/(\pi a^2)$, which is given in Table I for each of the three designs. The inverse relationship between pedestal temperature and pedestal density is a feature that is found in all of the models for the H-mode pedestal [2]. It is strongly supported by experimental evidence. For the pedestal model presented here, the product of pedestal density times pedestal temperature varies by less than 7% over the range considered in ITER, FIRE, and IGNITOR.

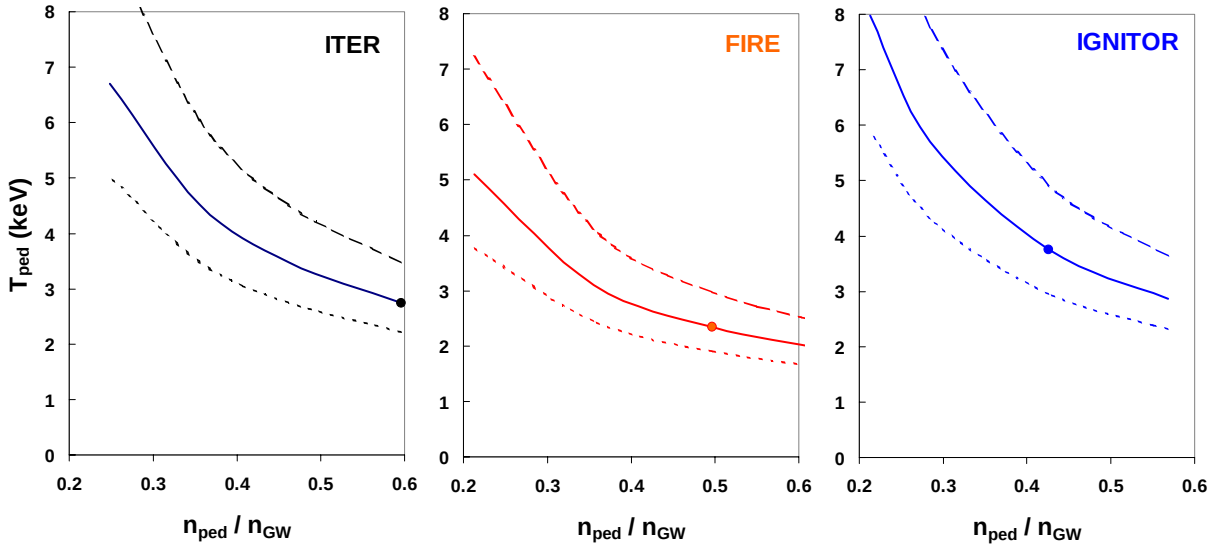


*Fig. 6: Pedestal temperature as a function of pedestal density normalized by the Greenwald density for the ITER, FIRE, and IGNITOR designs. In each panel, the solid curve is computed using the standard model described in the previous section. The dashed curves are computed using models that are one standard deviation above and below the standard model. The solid point indicates the pedestal temperature at the pedestal density corresponding to the reference design plasma density.*

The predictive pedestal model yields a pedestal density that is proportional to the average plasma density, which can be varied by controlling the plasma fuelling. Fig. 7 shows the fusion $Q \equiv P_\alpha / P_{aux}$ as a function of the volume-averaged plasma density normalized by the Greenwald density for ITER, FIRE, and IGNITOR. Fig. 8 shows the alpha heating fraction $[P_\alpha/(P_\alpha+P_{aux}+P_\Omega)]$ from the same simulations. (In these definitions, $P_\alpha$ is the alpha heating power, $P_{aux}$ is the auxiliary heating power, and $P_\Omega$ is the Ohmic power at the end of each simulation.) These results were predicted by the BALDUR code using the standard Multi-Mode transport model [1] together with the model presented above for the pedestal density and temperature. The solid curve in each figure is produced from simulations using the standard pedestal model (as described above using $C_W = 2.42$). The dashed curves in each figure are produced using pedestal models that are one standard deviation above and below the standard model (ie, using $C_W = 4.86$ for the dashed curve above and $C_W = 1.16$ for the dashed curve below the standard model).

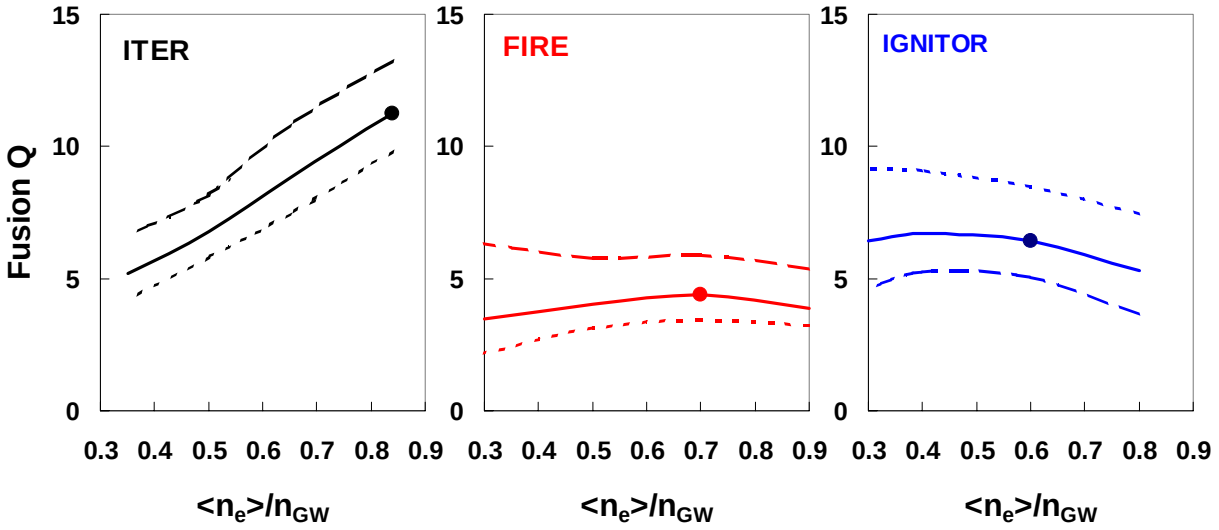


*Fig. 7: Fusion Q as a function of volume-averaged plasma density normalized by the Greenwald density for the ITER, FIRE, and IGNITOR designs. In each panel, the solid curve is computed using the standard model for the pedestal temperature described in the previous section. The dashed curves are computed using models that are one standard deviation above and below the standard model. The solid point indicates the fusion Q at the pedestal density corresponding to the reference design plasma density.*

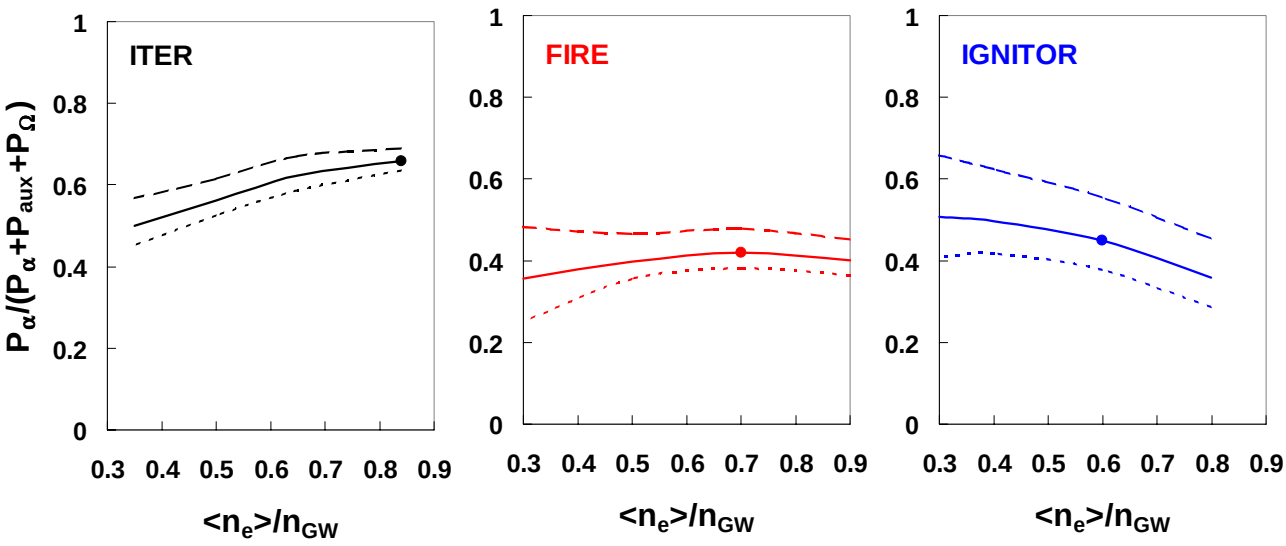


*Fig. 8: Alpha heating fraction as a function of volume-averaged plasma density normalized by the Greenwald density for the ITER, FIRE, and IGNITOR designs. In each panel, the solid curve is computed using the standard model for the pedestal temperature described in the previous section. The dashed curves are computed using models that are one standard deviation above and below the standard model. The solid point indicates the alpha heating fraction at the pedestal density corresponding to the reference design plasma density.*

In the simulations shown in Figs. 7 and 8, the auxiliary heating power is 40 MW for ITER, 30 MW for FIRE, and 10 MW for IGNITOR. With these levels of auxiliary heating power, the total heating power ($P_\alpha$+$P_{aux}$+$P_\Omega$) is safely above the heating power needed to make the transition from L-mode to H-mode($P_{L\rightarrow H}$ in Table I). It is found that the fusion $Q$ and alpha heating fraction increase as the auxiliary heating power is decreased in these simulations, as shown in Fig. 9. This behavior is one consequence of the stiffness of the transport model. There is strong evidence from both theory and experiment that the core transport model is "stiff", which means that the transport increases rapidly at any given point in the plasma with increasing logarithmic temperature gradient, once that temperature gradient rises above a threshold value. The Multi-Mode transport model used in these simulations is moderately stiff. Some transport models, such as the GLF23 model [5] are more stiff than the Multi-Mode model, while other transport models are less stiff.

There are a number of consequences resulting from the stiffness of the core transport. One consequence is that the core temperature profile, and therefore the fusion heating power, increases with increasing H-mode pedestal temperature. Another consequence of the stiffness of the core transport is that the transport provides strong burn control, since small increases in fusion heating are rapidly offset by corresponding increases in the heat transport.Finally, it is found that the predicted fusion power can be

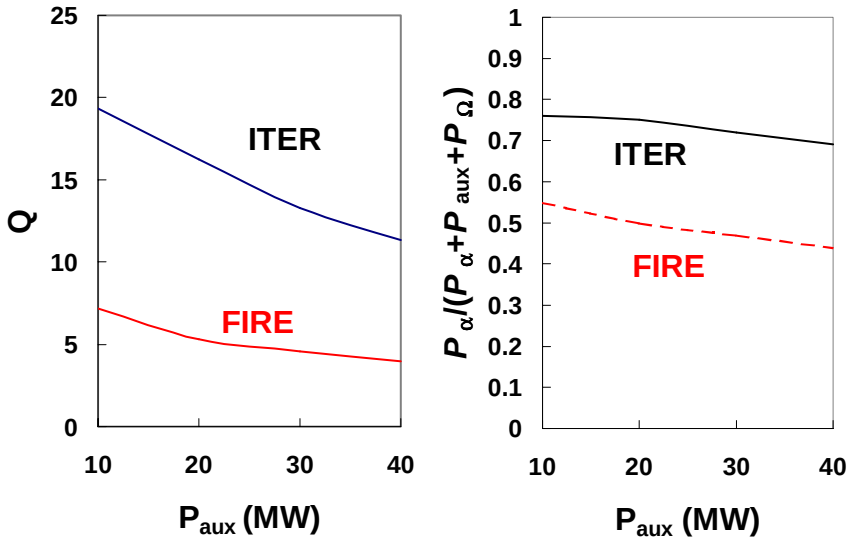


*Fig. 9: Fusion Q and fusion heating fraction as a function of auxiliary heating power for ITER and FIRE at the reference design point.*

increased by decreasing the impurity concentration in the plasma. This effect is illustrated in Fig. 10, in which carbon is used as the single impurity in the ITER design, rather than the more complicated design specification of 2% Beryllium plus 0.12% Argon plus the natural accumulation of helium.

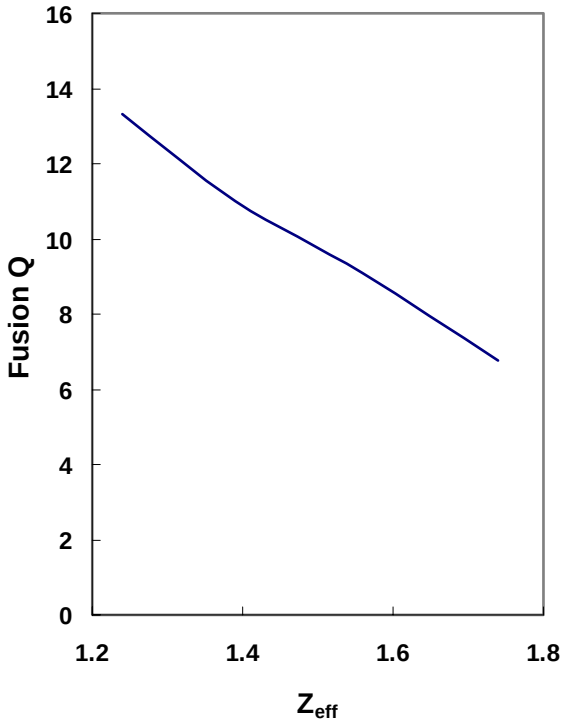


*Fig. 10: Fusion Q as a function of Zeff for the ITER design using carbon plus the natural accumulation of Helium as the only impurities.*

Charged particle transport and the resulting ion density profiles are computed in all the BALDUR simulations for the deuterium, tritium, and impurity ions. Particle transport is an integral part of the Multi-Mode transport model. The density profiles, however, are tightly constrained in these H-mode simulations by the condition that the pedestal density is 71% of the average plasma density. Typically, the peak density is about 10% higher than the volume-averaged density. In some simulations, there is a slight hollowness to the central density profile, with an annular ring of higher density. The deuterium-tritium fusion reactions in these simulations produce an accumulation of Helium that is balanced by diffusion to the edge of the plasma, where the Helium is assumed to be pumped away. The resulting Helium concentration is less than 2% of the electron density in nearly all of the simulations.

## Conclusions:

A predictive model has been developed for the temperature and density at the top of the pedestal at the edge of type 1 ELMy H-mode plasmas. The pedestal temperature from this model is nearly inversely proportional to the pedestal density. The pedestal model has been used together with the Multi-Mode model in simulations to predict the performance H-mode plasmas of the ITER, FIRE, and IGNITOR designs.

It should be kept in mind that the Multi-Mode core transport model and the H-mode pedestal model used in these simulations were calibrated extensively using experimental data from standard H-mode discharges.

## Acknowledgments

We thank Drs. G. Hammett and V. Parail for their contributions to the pedestal model and the research presented here.

## References:

1 Glenn Bateman, Arnold H. Kritz, Jon E. Kinsey, Aaron J. Redd and Jan Weiland, Phys. Plasmas **5** (1998) 1793-1799.

2 T. Onjun, G. Bateman, A. H. Kritz, and G. Hammett, “Models for the pedestal temperature at the edge of H-mode tokamak plasmas,” submitted to Physics of Plasmas.

3 A.H. Kritz, G. Bateman, T. Onjun, A. Pankin, and C. Nguyen, " Testing H-mode Pedestal and Core Transport Models Using Predictive Integrated Modeling Simulations," Proceedings of the 2002 European Physical Society Meeting, 2002.

4 C. E. Singer, D. E. Post, D. R. Mikkelsen *et al.*, Computer Physics Communications **49** (1988) 275-398.

5 J.E. Kinsey, G.M. Staebler and R.E. Waltz, Phys. Plasmas **9** (2002) 1676-1691.

6 D. Hannum, G. Bateman, J. Kinsey, A. H. Kritz, T. Onjun, and A. Pankin, Phys. Plasmas **8** (2001) 964-974; T. Onjun, G. Bateman, A. H. Kritz, and D. Hannum, Phys. Plasmas **8** (2001) 975-985; A. Pankin, G. Bateman, A. H. Kritz, M. Greenwald, J. Snipes, and T. Fredian, Phys. Plasmas **8** (2001) 4403-4413.

7 M. Sugihara, Y. Igitkhanov, G. Janeschitz, *et al.*, Nuclear Fusion 40 (2000) 1743.

8 F. Bombarda, IAP Seminar, PSFC, January 16th 2002, see web page http://www.frascati.enea.it/ignitor/.